European Journal of Pharmaceutics and Biopharmaceutics 142 (2019) 247–257

Contents lists available at ScienceDirect

European Journal of Pharmaceutics and Biopharmaceutics

journal homepage: www.elsevier.com/locate/ejpb

Research paper

Platelet lysate loaded electrospun scaffolds: Effect of nanofiber types on wound healing

Leticia Malgarim Cordenonsi[a,1], Angela Faccendini[b,1], Silvia Rossi[b], Maria Cristina Bonferoni[b], Lorenzo Malavasi[c], Renata Raffin[a], Elfrides Eva Scherman Schapoval[a], Claudia Del Fante[d], Barbara Vigani[b], Dalila Miele[b], Giuseppina Sandri[b,*], Franca Ferrari[b]

[a] Laboratório de Controle de Qualidade Farmacêutico/Faculdade de Farmácia, Universidade Federal do Rio Grande do Sul (UFRGS), Av. Ipiranga, Porto Alegre, Brazil
[b] Department of Drug Sciences, University of Pavia, Viale Taramelli 12, 27100 Pavia, Italy
[c] Department of Chemistry, Physical Chemistry, University of Pavia, vialeTaramelli 12, 27100 Pavia, Italy
[d] Immunohaematology and Transfusion Service, Apheresis and Cell Therapy Unit, Fondazione IRCCS Policlinico S. Matteo, Viale Golgi 19, 27100 Pavia, Italy

ARTICLE INFO

Keywords:
Electrospinning
Pullulan
Alginate
Platelet lysate
Scaffolds
Wound healing

ABSTRACT

In healthy individuals, wound healing is a highly efficient process. However, interruptions of normal healing give rise to chronic wounds, characterized by inflammation with impaired angiogenesis and re-epithelialization. The aim of this work was the design and the development of electrospun nanofibrous scaffolds based on sodium alginate (SA) and pullulan (PUL) and loaded with human platelet lysate (PL) intended for skin reparation, to take the advantage of nanofibrous scaffolds (with improved physical structure) and of SA as biopolymer.

Two preparation approaches have been used to load PL in the scaffolds: as component of the PUL/SA matrix, to be electrospun, or as coating component, to cover the previously prepared electrospun PUL based membranes. A preformulation study to assess pullulan entanglement concentration and alginate or citric acid critical concentration, to obtain electrospun nanofibers, has been performed. The preparation process allowed to obtain insoluble systems starting from aqueous solutions and these were able to act as scaffolds for tissue engineering with suitable mechanical properties and PL release.

PL loading in PUL/SA matrix nanofibers did not substantially modify the nanofiber morphology before crosslinking, while the crosslinking process, in presence of PL, determined less sharp nanofibers probably due to an increase in hydrophilicity caused by PL proteins. On the contrary, the coated nanofibers showed an increase in diameters due to PL loading.

The two different approaches affected the fiber dimension and scaffold elasticity, especially for PL loaded systems. Anyhow, these differences were not crucial for fibroblast adhesion and proliferation which were mainly influenced by PL loading.

In particular, fibroblasts presented different conformation and orientation mainly due to the presence of PL. This caused a cell random orientation compatible to a fibroblast-to-myofibroblast transition that could enhance wound healing.

1. Introduction

In healthy individuals, wound healing is a highly efficient process. However, interruptions of normal healing give rise to chronic wounds, leading to approximately 40 million of patients worldwide and high financial burden on health care systems, and/or to abnormal healing with scar formations. No cure currently exits for chronic wounds, although recently terrific progress leads to significant advances in delineating factors involved in normal and pathological tissue repair, in wound healing treatment and patient care [1]. Normal wound healing occurs in four sequential and partially overlapping phases, thus including haemostasis, inflammation, proliferation, and remodelling: the components of the extracellular matrix (ECM) have a pivotal role to coordinate the complex biochemical events in tissue repair that involve interactions among cells, ECM components, and signalling compounds [2,3].

* Corresponding author at: Department of Drug Sciences, University of Pavia, Viale Taramelli 12, 27100 Pavia, Italy.
E-mail address: giuseppina.sandri@unipv.it (G. Sandri).
[1] The authors equally contributed to the paper.

https://doi.org/10.1016/j.ejpb.2019.06.030
Received 23 January 2019; Received in revised form 17 May 2019; Accepted 28 June 2019
Available online 29 June 2019
0939-6411/

Chronic wounds are characterized by a chronic, persistent inflammation with impaired angiogenesis and re-epithelialization, dysregulated cytokines/growth factors, and/or increased proteases activity, which delay normal progression of wound healing. Chronic ulcers (diabetic, vascular, pressure and age-related ulcers) are the product of chronic wounds: these are embedded in a surrounding fibrotic microenvironment and do not spontaneously close.

Split-thickness autografts, despite being considered the gold standard due to the capability to accelerate wound healing and to prevent immune rejection, have morbidity, and pain at donor site. For these reasons in regenerative medicine, tissue engineering plays an important role and scaffolds based on biomaterials have been described as effective support to enhance ulcer healing [4,5].

Moreover, recently, hemoderivatives have been proposed as therapeutic tool to accelerate wound healing and to recovery chronic wounds. In particular platelet lysate (PL), from lysis of hyperconcentrate platelet suspension, is a pool of bioactive components, especially growth factors (GFs), involved in tissue regeneration. The PL contains PDGF (platelet derived growth factor), TGF-β, PDEGF (platelet derived epidermal growth factor), EGF (epidermal growth factor), VEGF (vascular endothelial growth factor), FGF, IGF, IL-8, and TNF-α and proved to be effective in tissue regeneration by accelerating fibroblast proliferation, keratinocyte migration, by activating an inflammatory cascade and due to its antimicrobial properties [6–8].

Given this premises, the aim of this work was the design and the development of nanofibrous scaffolds based on sodium alginate (SA) and pullulan (PUL) and loaded with human PL intended for skin reparation. Several strategies have been explored to manufacture scaffolds. Among various approaches, electrospinning is simple and effective and allows to obtain nanofibrous scaffolds starting from polymeric blends by means of high constant electric field between a needlepoint capillary tip and a collector [9–11]. Several polysaccharides have been investigated with respect to their ability to form fibres using electrospinning, considering that their physicochemical properties affect nanofibrous scaffold morphology, mechanical properties, degradation, cell adhesion, and proliferation [12–16].

In this work PUL (a linear polysaccharide, constituted of repeating units of α-(1 → 6)-linked maltotriose, with three glucopyranoses units linked by α-(1 → 4) glycosidic bonds) has been selected due to the ease of electrospinning, its thermal stability, and biocompatibility [17–19]. As PUL, SA (a linear polysaccharide derived from marine brown algae and based on (1–4) linked β-D-mannuronic acid (M) and α-L-glucuronic acid (G) units) is characterized by biocompatibility and biodegradability, moreover depending on G/M ratio it could be crosslinked with divalent ions (especially Ca^{2+}) forming hydrogels with the well-described egg-box structure. It is widely used in many biomedical applications, although it is not described as electrospinnable polymer [20,21].

Two different approaches have been considered: PL loading into the nanofiber polymeric matrix and PL loading in the nanofiber coating.

2. Materials and methods

2.1. Materials

The following polysaccharides were used. Pullulan (PUL) low MW ~ 200000–300000 Da (food grade, Hayashibara, Japan, Giusto Faravelli, Italy) and low molecular weight (SA) and medium molecular weight (mSA) sodium alginate (Sigma Aldrich, Italy) were chosen.

Platelet lysate (PL) was obtained from the Apheresis Service of Immunohaematology and Transfusion Service Centre for transplant immunology, by employing a sterile connection technique. Aliquots of hyper-concentrate platelets (high platelet concentration in small plasma volume and minimal leukocyte contamination) were obtained from apheresis, carried out on regular blood donors (Immunohaematology And Transfusion Service, Apheresis and Cell Therapy Unit, Fondazione IRCCS Policlinico S. Matteo, Pavia, Italy). The platelet pool was frozen at −80 °C for 5 h and subsequently unfrozen in a sterile water bath at 37 °C. An automated platelet count and tests for aerobic, anaerobic and fungi contamination were performed after saline dilution.

As crosslinking agents, citric acid (CA) and calcium chloride ($CaCl_2$) (Sigma Aldrich, Italy) were used.

Ultrapure water was obtained from a Milli-Q apparatus (Millipore®, Italy). All other chemicals were of analytical grade and used as received.

2.2. Methods

2.2.1. Evaluation of pullulan entanglement concentration

Pullulan was hydrated in distilled water at different concentrations ranging from 2.5 to 22% w/w. The rheology measurements were carried out by means of a rotational rheometer (MCR 102 rheometer, Anton Paar, Torino, Italy) at 28 °C, using a cone plate combination (C35/1: 35.0 mm diameter and 1° angle) as the measuring system. The rheological measurements were performed after 3 min of rest time. Curves of shear stress vs shear rate (flow curves) were plotted and η_0 and η_∞ were calculated as the angular coefficient of the tangent in the first part and in the last part of flow curves, respectively [22]. Profiles of η_0 and η_∞ vs pullulan concentration were plotted and the intersection between the two curves was identified as entanglement concentration [22].

2.2.2. Scaffolds development

2.2.2.1. Evaluation of electrospinnability. Pullulan was hydrated in distilled water at different concentrations from 7,5 to 22% w/w. 20% w/w pullulan concentration was selected. Subsequently two different types of polymer blends based on pullulan and alginate were considered: the first type was based on medium MW alginate, while the second one on low MW alginate. As for medium MW alginate, three types PUL/mSA scaffolds were prepared starting from the following polymer blends: PUL/mSA 20/1%, 20/1.5%, 20/2% and 20/2.5% w/w. As for low MW alginate, PUL/SA scaffolds was obtained starting from 20/5% w/w blend. In particular PUL was dissolved in ultrapure water under continuous stirring for 3 h, subsequently SA was added under continuous stirring for further 2 h at room temperature (25 ± 2 °C).

PUL/mSA 20/2% w/w and PUL/SA 20/5% w/w were subjected to viscosity measurements as previously described, considering shear stress ranging from 10 to 1000 s^{-1}.

Pullulan was hydrated in distilled water at 20% w/w in presence of 2,5 and 5% w/w of citric acid, as crosslinking agent [23]: these membranes were prepared as the core structures (PUL/CA) to be coated with alginate in the coated scaffolds. At this purpose PL was hydrated in 5% w/w CA aqueous solution under continuous stirring for 3 h at room temperature (25 ± 2 °C).

PUL/SA and PUL/CA solutions were freshly prepared, just before electrospinning. The process was performed at 28–32% relative humidity and 25–28 °C temperature.

All the polymer blends were subjected to electrospinning using an instrument (STKIT-40, Linari Engineering, Italy) equipped with a syringe fitted with a metallic needle (inner diameter of 0.8 mm). A syringe pump was used to feed it at a constant rate. High voltage at the needle was achieved by connection to a voltage generator (Model R-99E, Razel TM, Linari Engineering, Italy) capable of generating voltages in the range of 0–40 kV. A plastic stand wrapped with aluminium foil was used as a collector. The electrospinnability was evaluated modulating voltage from 15 to 24 kV, and needle to collector distance from 15 to 20 cm.

The nanofiber morphology was assessed as by SEM (Tescan, Mira3XMU, CISRIC, University of Pavia). Samples were mounted on metal stubs using a double-sided adhesive tape and sputter-coated by means of gold deposition under vacuum.

Table 1
Quali-quantitative compositions of polysaccharide solutions to obtain nanofibrous scaffolds.

	Pullulan PUL (% w/w)	Sodium alginate SA (% w/w)	Citric acid CA (%)	Distance (cm)	Voltage (kV)	Flow (ml/h)
PUL/SA	20	5	–	15	28	0.2
PUL/CA	20	–	5	24	22	0.1

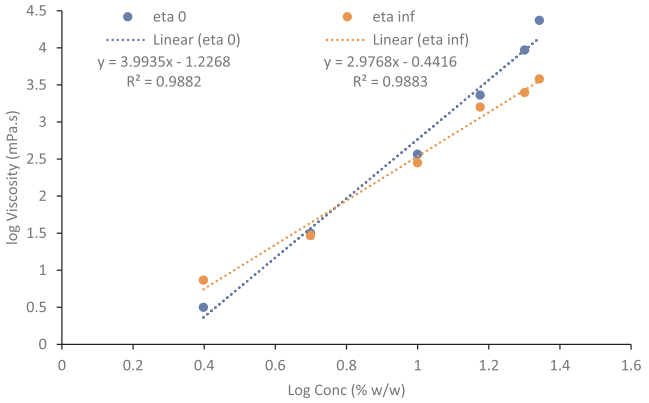

Fig. 1. Log viscosity of n0 and n∞ vs log concentration (% w/w) profiles evaluated for pullulan solutions ranging from 2.5 to 22% w/w. In the legend the linear fitting is reported. The englament concentration (intersection between log viscosity of n_0 vs log pullulan concentration with log viscosity of n_∞ vs log pullulan concentration is 5.9% w/w.

2.2.2.2. Crosslinking of nanofibrous scaffolds. PUL/SA scaffolds were removed from the collector plate and crosslinked by dipping the scaffolds in $CaCl_2$ solution (5% w/w) in absolute ethanol for 2 h, and subsequently by rinsing them in ultrapure water for 1 min.

PUL/CA scaffolds were crosslinked by heating at 150 °C for 1 h. Subsequently the scaffolds were dipped in 5% w/w SA aqueous solution for 1 h, and then dipped in $CaCl_2$ aqueous solution (5% w/w) for 1 h and washed for 1 min to eliminate the excess of Ca^{2+}. 0.1 g/cm^2 SA solution was used.

2.2.3. Optimized systems

2.2.3.1. Characterization of polymer blends. Table 1 reports the quali-quantitative compositions of the selected systems.

The polymer blends used for the selected systems were deeply characterized for pH, conductivity, surface tension, and rheology.

The pH values of the polysaccharide solutions were determined using pHmeter (model pH 210 m, Hanna Instruments, Italy) at 25 ± 0.5 °C.

The conductivity of polysaccharide solutions was measured using a conductometer (FiveGo FG3 Portable Conductometer, Mettler Todelo, Italy). The probe was calibrated with a standard solution (1413 μS/cm) prior to use.

The surface tension was assessed using a tensiometer (DY-300 –

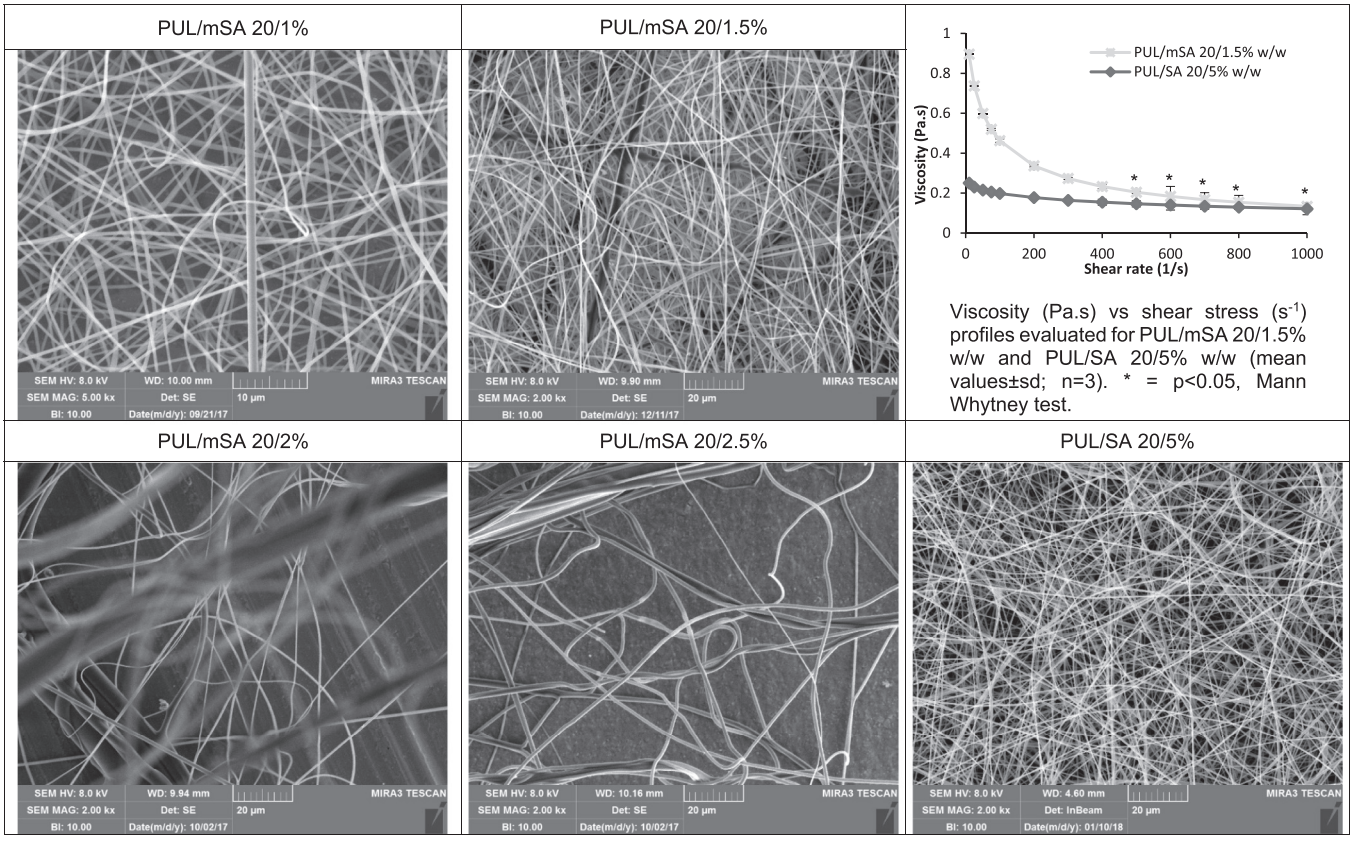

Fig. 2. SEM microphotographs of pullan and medium molecular weight alginate nanofibers (PUL/mSA) prepared starting from pullulan solution at 20% w/w with different concentrations of alginate and pullulan and low molecular weight alginate nanofibers prepared starting from pullulan solution at 20% w/w with 5% w/w Alginate (PUL/SA 20/5% w/w). In the inset, the viscosity (Pa s) vs shear stress (s^{-1}) profiles evaluated for PUL/mSA 20/1.5% w/w and PUL/SA 20/5% w/w are reported. * = $p < 0.05$, Mann Whitney test.

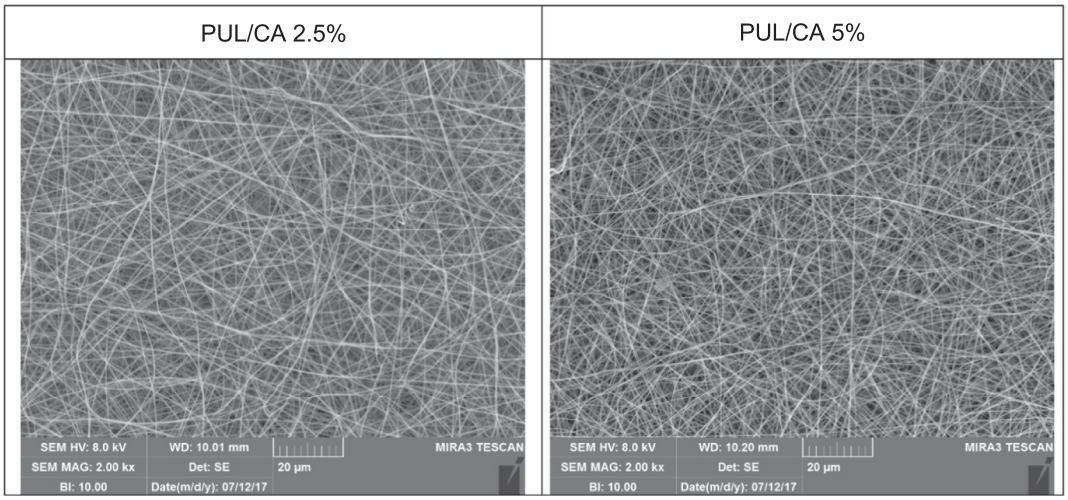

Fig. 3. SEM microphotographs of pullan and citric acid nanofibers (PUL/CA) prepared starting from pullulan solution at 20% w/w with different concentrations of citric acid.

Table 2
Chemico-physical properties of polysaccharide solutions (mean values ± sd; n = 3).

	PUL/SA	PUL/CA
pH	7.23 ± 0.01	1.29 ± 0.01
Conductivity (µS/cm)	1945.67 ± 2.96	1488.75 ± 2.39
Surface tension (mN/m)	45.16 ± 0.31	71.14 ± 1.16
Viscosity (Pa s)	13.58 ± 1.90	2.12 ± 1.32

Kyowa, Japan) with a measurement range between 0 and 100 mN/m. Measurements were carried out at 25 °C by a time-based detection.

The rheological analysis was carried out as previously described at 28 °C. The apparent viscosity was determined at 200 s^{-1}.

2.2.3.2. PL loading. As for PUL/SA/PL scaffolds, PL was loaded into nanofiber polymeric matrix. PL (16.7% w/w) was added to polymer solution PUL/SA before electrospinning process. The electrospinning parameters were the same used for PUL/SA.

As for PUL/CA coated with SA/PL scaffolds, PUL/CA was electrospun and crosslinked as previously described. Subsequently the nanofibers were coated by dipping using 5% w/w SA and 16.6% w/w PL aqueous solution for 1 h, and then coated nanofibers were immersed in 5% w/w $CaCl_2$ aqueous solution for 1 h, to obtain the crosslinking and washed in ultrapure water for 1 min to eliminate the excess of Ca^{2+}. 0.1 g/cm^2 SA solution was used.

2.2.3.3. Characterization of nanofibrous scaffolds

2.2.3.3.1. Chemico-physical characterization. The morphology of the nanofibrous scaffolds were analyses as previously described and the scaffolds were analysed before and after crosslinking and without and with PL loading. Fiber dimensions were evaluated by means of an image analysis software (Meazure 2.0 software, C Thing Software, USA) from the SEM images and at least 30 nanofibers were randomly selected).

FT-IR analysis were carried out by means of Infrared Imaging Microscope (Nicolet iN10 MX, Thermo Scientific). The infrared spectra were acquired over a wavenumber range of 4000–500 cm^{-1} at a resolution of 10–20 μm^2.

2.2.3.3.2. Mechanical properties. Mechanical properties of nanofibrous scaffolds were measured using a TA-XT plus Texture Analyzer (Stable Microsystems, ENCO, Italy) equipped with a 5.0 kg load cell. Before testing, nanofibrous scaffolds were cut 30 × 10 mm and the strips obtained were clamped between tensile grips A/TG probe, setting an initial distance between the grips of 20.0 mm. Then, the upper grip was raised at a constant speed of 5.0 mm/s up to a distance equal to 20.0 mm, corresponding to 100% elongation. Nanofibrous scaffolds were visually inspected in order to observe the occurrence of a physical damage (break) during the test. % elongation corresponding to scaffold break was recorded together with the related tensile strength applied (force at break) (TS, N/mm^2). The initial linear region of stress vs strain curves was fitted. Young modulus (index of scaffold elasticity) was the angular coefficient of each fitted line.

2.2.3.3.3. PL loading and release. PL loading and release were assessed by dosing the total amount of proteins by means of Bredford assay. PL was assayed as such, and after lyophilization and resolubilization, to determine the total amount of proteins.

PL loading in the scaffolds was assessed as follows.

As for the PUL/SA/PL scaffold, the amount of proteins loaded was assayed in the polymeric blend before electrospinning process and after solubilization of the scaffold before crosslinking. As for PUL/CA coated with SA/PL scaffold, the amount of PL associated to the scaffolds was calculated as the difference between the amount of proteins before the coating procedure, in the coating solution, and the amount remained in the coating solution after the coating and crosslinking process.

The scaffolds were accurately weighed and put in contact with distilled water as releasing medium. At pre-determined time intervals (1, 2 and 24 h), 20 µl of dissolution medium was collected and blended with 180 µl of Bradford reagent (Sigma-Aldrich, Italy). The absorbance of each sample was determined at 570 nm (absorbance of Coomassie Brillant blue dye) by means of ELISA plate reader (iMark® Microplate reader, Bio-Rad Laboratories SrL, Italy). Protein concentration was determined using the calibration curve. At this purpose, five aqueous solutions of bovine serum albumin (as standard) (Sigma-Aldrich, Italy) were considered (concentration range from 1 to 7.5 µg/ml). The method was linear in the concentration range considered ($R^2 > 0.995$).

2.2.4. Biopharmaceutical characterization

2.2.4.1. In vitro biocompatibility. Fibroblasts (from juvenile foreskin (PromoCell GmbH, VWR, Italy) were cultured in presence of Dulbecco's modified Eagle medium (Sigma-Aldrich, Italy) and supplemented with 10% fetal calf serum (FCS, Euroclone, Italy) with 200 IU/ml penicillin and with 0.2 mg/ml streptomycin (Sigma-Aldrich, Italy), kept at 37 °C in a 5% CO_2 atmosphere with 95% relative humidity (RH).

Fibroblasts were seeded onto nanofibrous scaffolds (area 0.36 cm^2 – diameter 0.2 cm), placed in 96-well plate bottom wells. Fibroblast

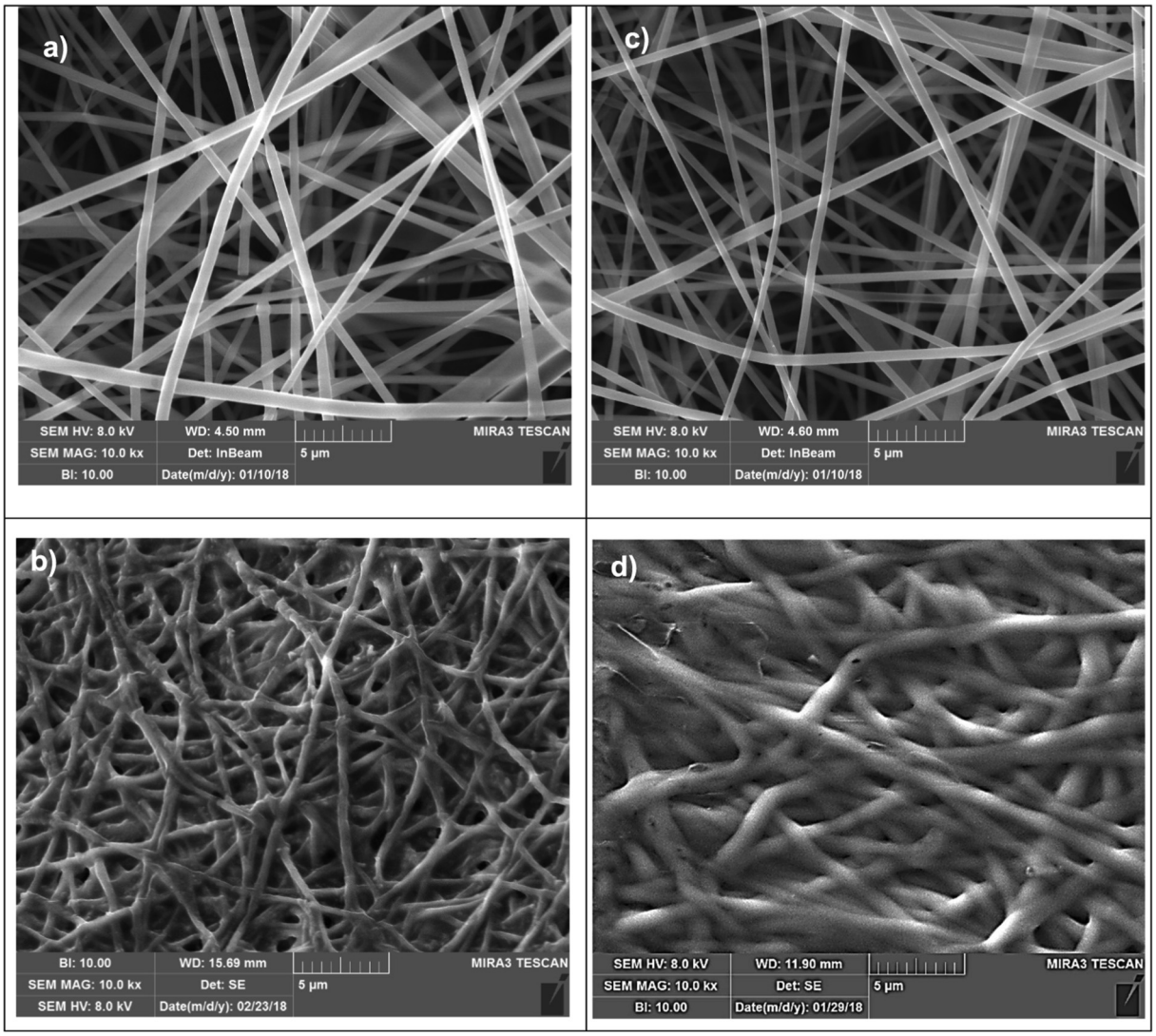

Fig. 4. SEM microphotographs of (a) PUL/SA, (b) PUL/SA crosslinked, (c) PUL/SA/PL, (d) PUL/SA/PL crosslinked.

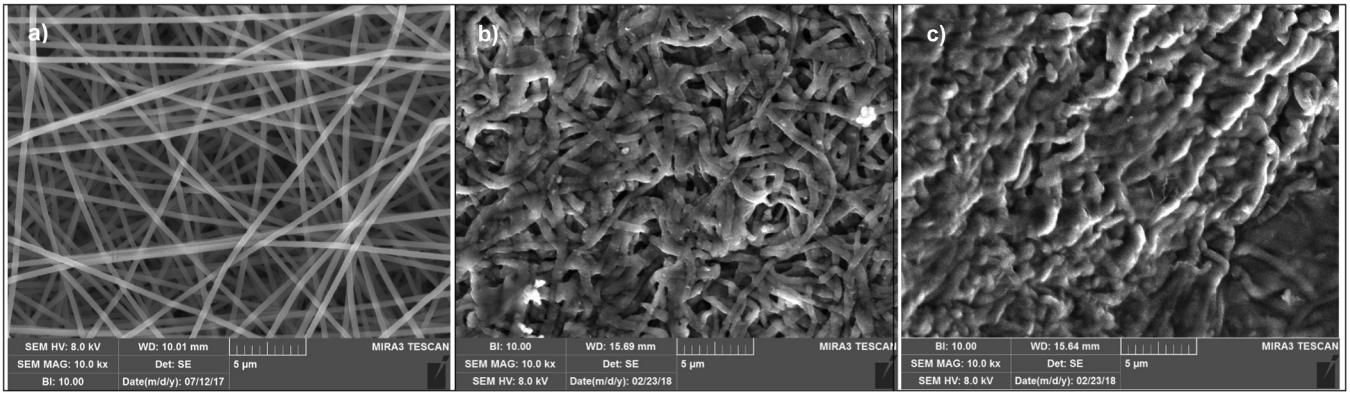

Fig. 5. SEM microphotographs of (a) PUL/CA; (b) PUL/CA coated with SA; (c) PUL/CA coated with SA/PL.

density was 10^5 cells/cm^2. As reference, fibroblasts grown in standard conditions were considered (10^5 cells/cm^2 seeded in each well). To evaluate cell adhesion and proliferation, MTT assay was performed after 3 and 6 days of growth.

Cell medium was removed from each well and 150 µl MTT (3-(4,5-dimethylthiazol-2-yl)-2,5-diphenyltetrazolium bromide, Sigma-Aldrich, Italy) solution in DMEM without phenol red (Sigma-Aldrich, Milan, Italy) (0.8 mg/ml concentration) were added to each well and incubated for 3 h. MTT reagent was removed from each well and finally, 100 µl of dimethyl sulfoxide (DMSO, Sigma-Aldrich, Italy), as solubilizing agent, was added. The optical density was measured by means of an ELISA plate reader at a wavelength of 570 nm and 690 nm (reference wavelength) after 60 s of mild shaking. Results were expressed as % ratio between the absorbance for each scaffold and the reference

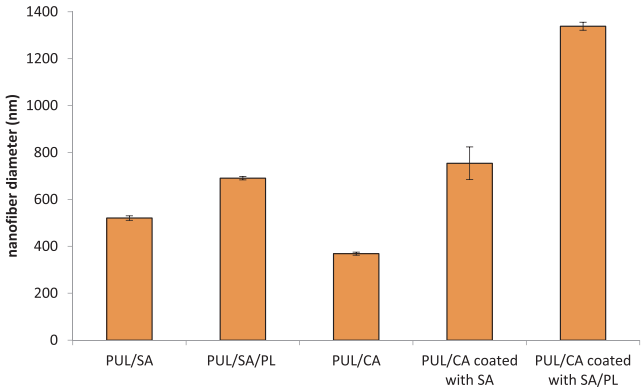

Fig. 6. Nanofiber diameters (nm) measured for PUL/SA and PUL/CA and PUL/CA coated with SA scaffold, unloaded and loaded with PL (mean values ± sd; n = 30).

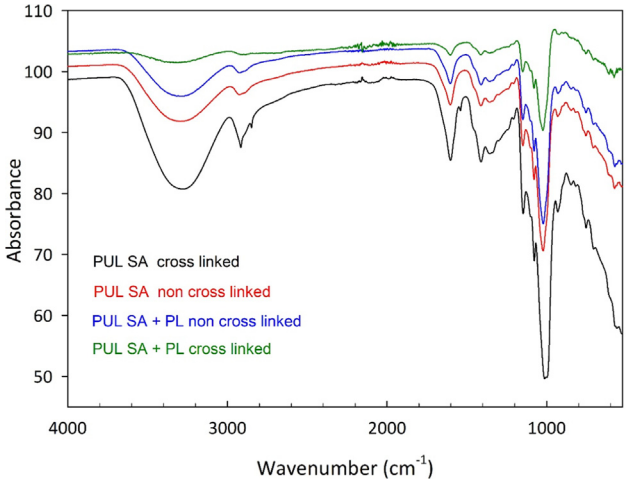

Fig. 7. FTIR spectra of PUL/SA scaffolds: (a) PUL/SA, (b) PUL/SA crosslinked, (c) PUL/SA/PL, (d) PUL/SA/PL crosslinked.

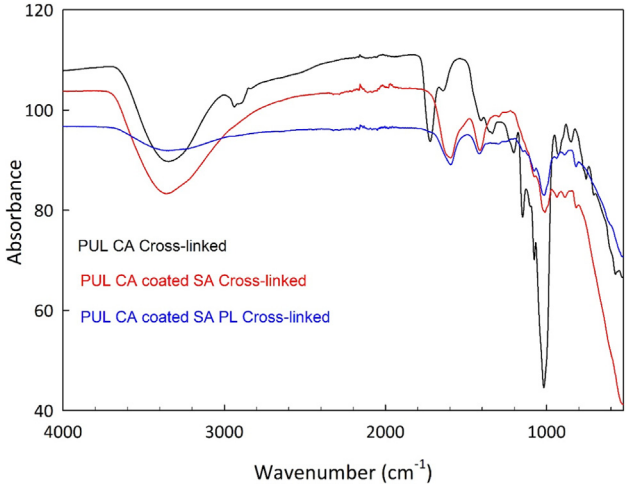

Fig. 8. FTIR spectra of (a) PUL/CA; (b) PUL/CA coated with SA; (c) PUL/CA coated with SA/PL.

(standard growth conditions). Thus, the optical density of the reference (standard growth conditions) was considered as 100%.

2.2.4.2. CLSM analysis. The cells grown onto the scaffolds (6 days of growth) were fixed using a 3% (*w/v*) glutaraldehyde solution in PBS (Sigma-Aldrich, Italy) for 1 h at 5 °C. The substrates were then washed three times with PBS containing 5% w/w $CaCl_2$.

Cellular cytoskeleton was stained by incubating with 50 µl (50 µg/ml) phalloindin-Atto 488 (Sigma-Aldrich, Italy) for 40 min, in the dark. Then, each substrate was washed twice, and cell nuclei were stained with 100 µl of Hoechst 33258, diluted 1:10000 (Sigma-Aldrich, Italy), for 15 min in the dark.

Scaffolds were placed on a microscope slide and imaged using a Confocal Laser Scanning Microscope (CLSM, Leica TCS SP2, Leica Microsystems, Italy) with λex = 346 nm and λem = 460 nm for Hoechst 33258 and λex = 501 nm and λem = 523 nm for phalloindin-Atto 488.

The acquired images were processed with software associated with the microscope (Leica Microsystem, Italy).

2.2.5. Statistical analysis

Statistical differences were evaluated by means of *t*-test, (Statgraphics Centurion XV, Statistical Graphics Corporation, MD, USA). Differences were considered significant at $p < 0.05$ and each p value is reported in the text or in the captions.

3. Results and discussion

3.1. Characterization of pullulan entanglement concentration and its electrospinnability

Fig. 1 reports the η_0 and η_∞ vs pullulan concentration profiles. The profiles were characterized by linear regression with R^2 higher than 0.988, to indicate a good linear fitting. The intersection point of the two profiles corresponded to 5.9% w/w of pullulan concentration and this was identified as the entanglement concentration [22]. This was the lower concentration that could be considered to obtain a continuous liquid jet during the electrospinning process and consequently nanofibers. Preliminary electrospinning trials evidenced that 20% w/w pullulan solution was the lower concentration to obtain regular nanofibers without beads or any other defects (data not shown) and was selected as the optimal for the further preformulative study.

Fig. 2 reports SEM microphotographs of pullan and medium MW alginate nanofibers (PUL/mSA) prepared starting from pullulan solution at 20% w/w with different concentrations of alginate ranging from 1 to 2.5% w/w. The higher concentrations of alginate, 2 or 2.5% w/w, did not allow the preparation of homogeneous fibers that presented different dimensions and twisted pattern. As for the lower alginate concentrations, the nanofibers based on alginate concentrations in blends of 1 and 1.5% w/w were characterized by homogenous texture. Moreover, 1.5% w/w concentration allowed to obtain uniform nanofibers. However, upon crosslinking in presence of Ca^{2+}, this system remained water-soluble and not suitable to act as scaffold for tissue engineering. Thus, it was considered to decrease the molecular weight of alginate and to maintain the viscosity of the polymer blend (pullulan and low MW alginate), to be electrospun, superimposable to PUL/mSA 20/1.5% w/w. In Fig. 2 the viscosity (Pa*s) vs shear stress (s^{-1}) profiles evaluated for PUL/mSA 20/1.5% w/w and PUL/SA 20/5% w/w are reported. The blends were characterized by pseudoplastic profiles and their viscosity was superimposable for shear stress higher than 500 s^{-1} (shear rates in place during the electrospinning process [24]). In fact the SEM analysis (Fig. 2) evidences that the PUL/SA 20/5% w/w scaffold was characterized by homogeneous fibers similar to those of PUL/mSA 20/1.5% w/w. Moreover, the crosslinking preliminary results evidenced that this systems could be rendered insoluble upon Ca^{2+} crosslinking and was selected for further characterizations.

Fig. 3 reports SEM microphotographs of pullan and citric acid nanofibers (PUL/CA) prepared starting from pullulan solution at 20% w/w with different concentrations of citric acid. Both the systems were characterized by homogeneous nanofibers without defects. However the preliminary evaluation of crosslinking to control the solubility resistance, evidenced that citric acid at 5% w/w in blend allowed to

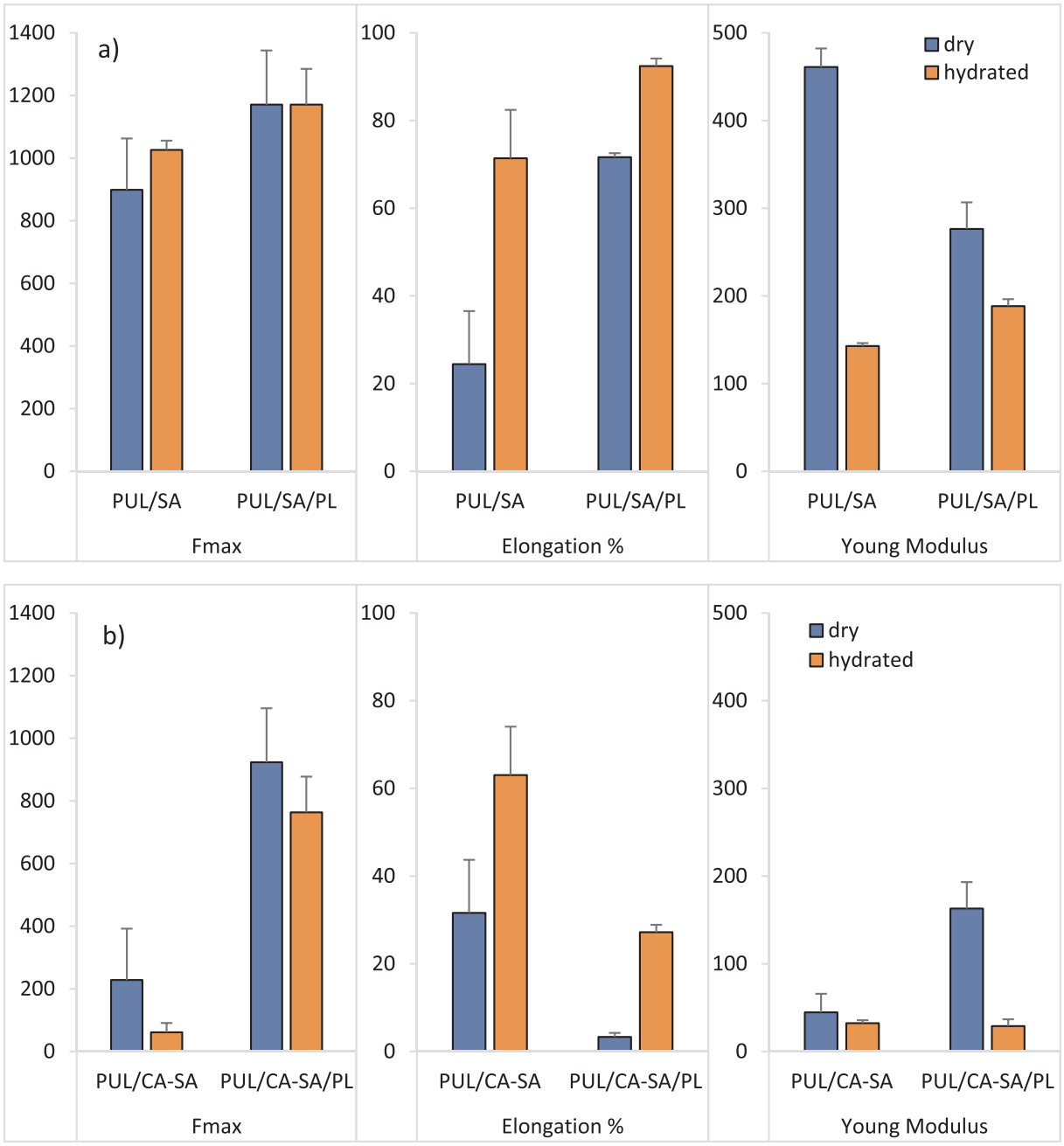

Fig. 9. Mechanical properties (Force at break – Fmax – mN/mm^2; elongation %; Young Modulus: mN/mm^2) evaluated for (a) PUL/SA and PUL/SA/PL scaffolds and (b) PUL/CA coated with SA and PUL/CA coated with SA/PL scaffolds (mean values ± sd; n = 3).

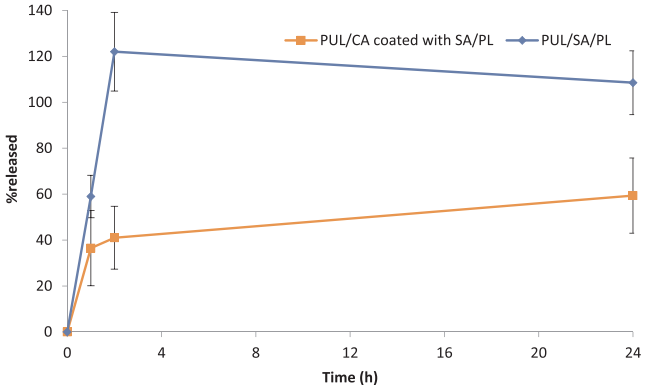

Fig. 10. Protein release profiles (mean values ± sd; n = 6).

prevent system solubilization and was selected for further characterizations.

3.2. Characterization of polysaccharide solutions

Table 2 reports pH, conductivity, surface tension, and viscosity evaluated for the selected blends, PUL/SA and PUL/CA. It is well known that the morphology and the diameter of electrospun nanofibers are directly related to components including polymer properties and intrinsic solution [25–29]. The two solutions prepared were characterized by significantly different chemico-physical properties. In particular pH, conductivity, surface tension, and viscosity of PUL/SA solution were significantly higher than those of PUL/CA. Generally, polymer solutions should have critical concentration to allow polymer chain entanglements and a surface tension high enough to have charge density able to

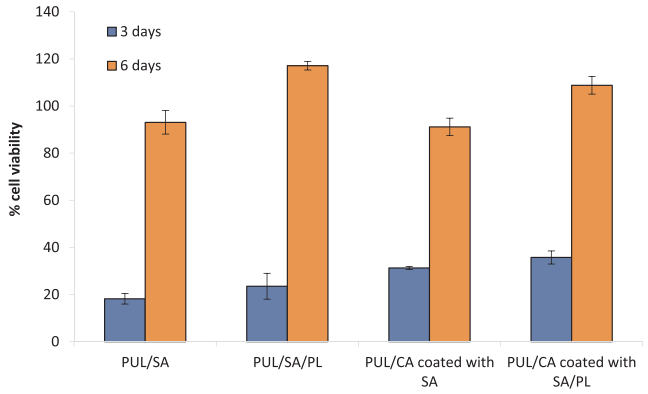

Fig. 11. Fibroblast % viability evaluated after cell growth onto PUL/SA and PUL/CA coated with SA unloaded and loaded with PL (mean values ± es; n = 8). (Statistics: Mann Whitney W test: PUL/SA 3 days vs PUL/SA/PL 3 days: p = 0.341; PUL/SA 3 days vs PUL/SA 6 days: p = 0.013; PUL/SA 6 days vs PUL/SA/PL 6 days: p = 0.565; PUL/SA/PL 3 days vs PUL/SA/PL 6 days: p = 0.004; PUL/CA coated SA 3 days vs PUL/CA coated SA 6 days: p < 0.001; PUL/CA coated SA PL 3 days vs PUL/CA coated SA 3 days: p = 0.145; PUL/CA coated SA PL 6 days vs PUL/CA coated SA 6 days: p = 0.183; PUL/CA coated SA PL 3 days vs PUL/CA coated SA PL 6 days: p < 0.001; PUL/SA/PL 3 days vs PUL/CA coated SA PL 3 days: p = 0.065; PUL/SA/PL 6 days vs PUL/CA coated SA PL 6 days: p = 0.944).

cause marked increase of Coulombic repulsion and electrostatic forces. These play an important role to have charged jet and to obtain a stretched and extended one able to form thinner fibres.

3.3. Chemico-physical characterization of scaffolds

Fig. 4 reports SEM microphotographs of PUL/SA scaffolds: (a) PUL/SA, (b) PUL/SA crosslinked, (c) PUL/SA/PL, and (d) PUL/SA/PL crosslinked.

Nanofibers were uniform and characterized by similar morphology and smooth surface (Fig. 4a) and the crosslinking process did not alter the nanofibrous structure, although the nanofibers showed an irregular and rough surface probably due to the rinsing step in distilled water to eliminate Ca^{2+} in excess (Fig. 4b). PL loading did not substantially modify the nanofiber morphology before crosslinking (Fig. 4c), while the crosslinking process in presence of PL determined less sharp nanofibers and this was probably due to the presence of PL proteins that could rendered the polymer matrix more hydrophilic and more sensitive to ethanol/water hydrophilicity (Fig. 4d).

Fig. 5 reports SEM microphotographs of (a) PUL/CA; (b) PUL/CA coated with SA, and (c) PUL/CA coated with SA and PL. Also in this case, nanofibers were uniform and characterized by smooth surface (Fig. 5a). The coating process caused a modification of nanofibrous structure and the fibres appeared partially blended although the fibre surface remained smooth and regular (Fig. 5b). PL loading further caused the nanofibers blending even though the nanofibrous structure remained visible (Fig. 5c). This behaviour was similar to that of PUL/SA/PL scaffolds, conceivably due to the increased hydrophilicity of the SA coating due to the presence of PL proteins.

Fig. 6 reports the nanofiber diameters in each scaffold. Considering PUL/SA nanofibers, the presence of PL determined a significative increase in fibre dimensions (from diameters of about 520 nm, for unloaded system, to diameters of about 680 nm, for PL loaded systems).

On the other hand, PUL/CA nanofibers showed diameters close to 370 nm, significantly lower than those of PUL/SA nanofibers. These results were in line with the physico-chemical properties of the corresponding solutions: the lower viscosity and higher surface tension of PUL/CA blend determined thinner nanofibers, while PUL/SA blend compensated higher viscosity and lower surface tension with higher conductivity [30,31].

The coating process of PUL/CA significantly increased fibre dimensions up to 750 nm. Moreover PL loading in SA solution determined a further significant increase of fibre dimensions in PUL/CA coated systems with fiber diameters up to 1300 nm. Similar results were obtained for PUL and pectin scaffolds by Liu et al. [32], where the crosslinking in Ca^{2+} solution caused a decrease in pore size and change in fibre morphology forming a tighter structure after scaffolds washing.

Fig. 7 reports FTIR spectra of PUL/SA scaffolds: (a) PUL/SA, (b) PUL/SA crosslinked, (c) PUL/SA/PL, and (d) PUL/SA/PL crosslinked and Fig. 8 reports the spectra of (a) PUL/CA; (b) PUL/CA coated with SA, and (c) PUL/CA coated with SA and PL.

The FTIR spectra of PUL/SA membranes either cross-linked or loaded with platelet lysate resembled each other and in particular they were all analogous to the FTIR spectra of cross-linked pullulan without appreciable differences in the signal positions and relative intensities. The spectrum of cross-linked pullulan was in agreement with previous literature reports [33] of polymerized pullulan showing the strong absorption peak of OH stretching at about 3305 cm^{-1} and sp3 C—H bond at 2940 cm^{-1}. Other features of pullulan were also observed in the spectra including C—O—H bend (1337 cm^{-1}) and C—O—C stretch (1152 cm^{-1}) (Fig. 7). Overall, this suggests that the spectra were dominated by the pullulan features.

FTIR spectra (Fig. 8) show a significant change passing from pure pullulan matrices to coated samples (with sodium alginate). The spectrum of pullulan membrane (uncoated scaffold) presented all the peculiar features of pullulan, as previously described. On the other hand, the spectra of the coated samples resulted to be characterized by less distinct features and with broad peaks. Both samples, irrespective by the presence of protein lysate, showed the superimposable spectra. A comparison with current literature suggests a close similarity of the present spectra with that of sodium alginate, characterized by absorption band characteristics at 3410 cm-^{1}, which could be due to hydroxyl group (—OH), 1635 cm^{-1} (asymmetric stretching vibration of COO groups), 1419 cm^{-1} (symmetric stretching vibration of COO groups), and 1050 cm^{-1} (elongation of C—O groups) [34].

3.4. Mechanical properties of scaffolds

Fig. 9 reports the results of scaffold mechanical properties as tensile strength (Fmax, mN mm), elongation (%) and Young modulus (mN/cm^2), measured in dry and hydrated scaffolds: (a) PUL/SA and PUL/SA/PL and (b) PUL/CA-SA and PUL/CA-SA/PL.

PUL/SA scaffolds were characterized by not significantly different forces at break (Fmax) in dry or hydrated state (Fig. 6a). PL loading slightly increased systems resistance to break, and this was particularly evident in hydrated state. Simultaneously, independently of PL loading, scaffolds based on PUL/SA were characterized by significantly greater elongation in hydrated state and PL loading determined a further increase of system deformation. This behaviour could be confirmed by the values of Young Module: hydrated systems showed greater elastic deformation while dry systems were stiffer, moreover the presence of PL caused a significant decrease of elastic deformation. PL loading of PUL/SA scaffolds affected system stiffness and the presence of PL increased system deformation and decreased their elasticity.

Analogously to that observed for PUL/SA scaffolds, PUL/CA coated SA scaffolds presented not significantly different forces at break (Fmax) in dry or hydrated state (Fig. 6b). PL loading significantly increased the system resistance to break, both in hydrated and in dry state. Simultaneously, scaffolds based on PUL/SA were characterized by elongation in hydrated state significantly greater than that of dry state, and PL loading determined a further significant decrease of system deformation, confirming their stiffness, although Young Modulus related to PUL/CA coated SA was not significantly different in dry or hydrated state. On the contrary PL loading scaffolds were characterized by significantly greater elasticity in dry state. In hydrated state (simulating the application environment) PL loading increased scaffold stiffness,

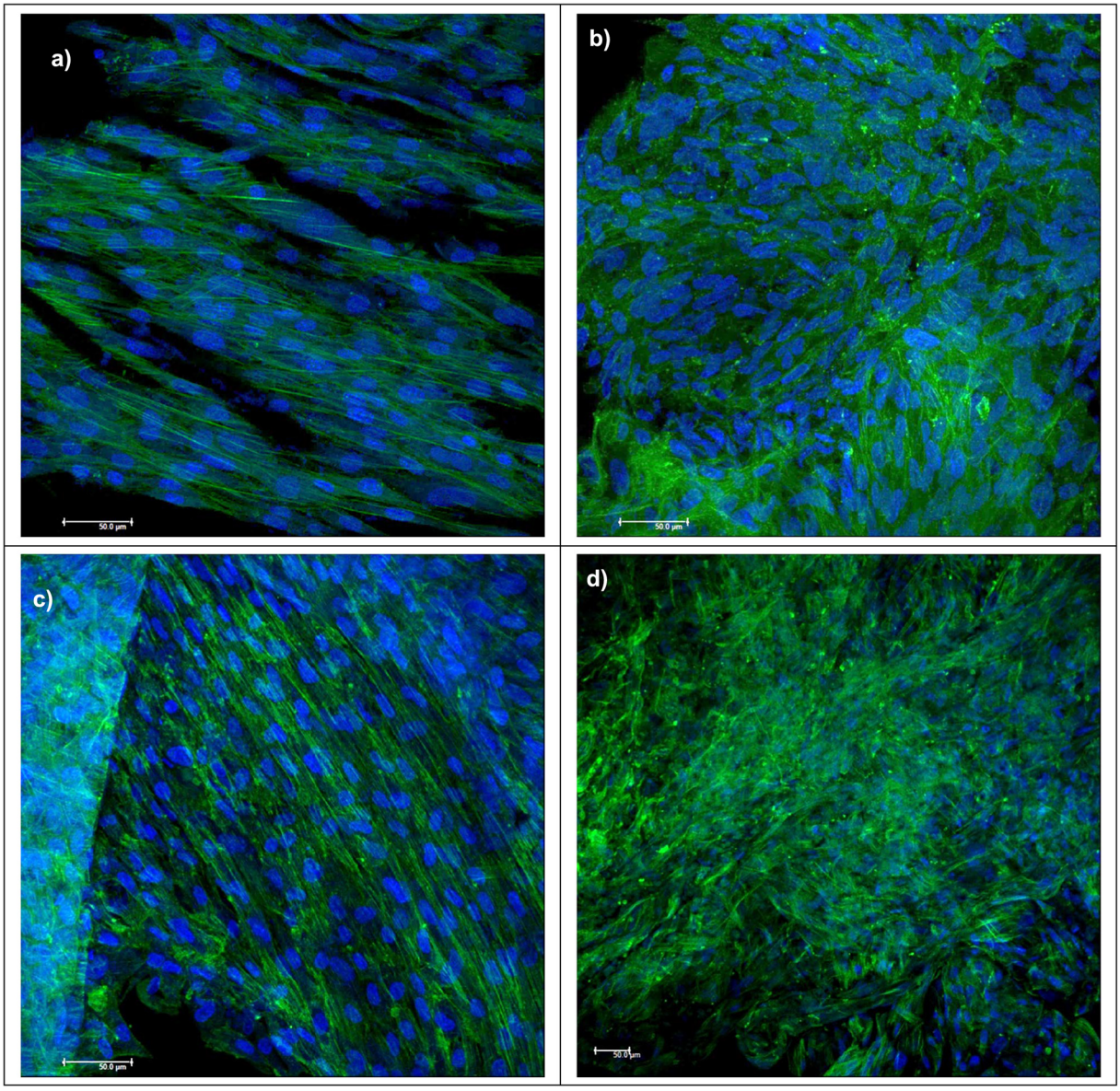

Fig. 12. CLSM microphotographs of fibroblasts grown onto (a) PUL/SA; (b) PUL/SA PL; (c) PUL/CA coated with SA; (d) PUL/CA coated with SA/PL (6 days of growth).

reducing their elasticity and their deformation. This behaviour, opposite than that evidenced for PUL/SA systems, could be due to the coating: this could determine a different consistency of fiber core based on PUL and CA and the coating based on SA gelled with Ca^{2+} in hydrated state.

3.5. PL loading and release

The content of proteins in PL before and after lyophilization remained the same and equal to 59 ± 4 mg/ml (mean values ± sd; n = 3). The PL loading of nanofibers was 3.5 ± 0.2% w/w (mean values ± sd; n = 3) for PUL/SA/PL and 12.8 ± 0.9% w/w (mean values ± sd; n = 3) for PUL/CA-SA/PL.

Fig. 10 reports the protein release from scaffolds. The PUL/SA/PL was characterized by a fast release during the first 2 h and it reached the plateau value at 100% of proteins released in 24 h. On the other hand, the PUL/CA-SA/PL scaffolds showed a lower release profiles and almost the 40% of proteins was liberated after 2 h and 60% after 24 h. The differences in protein release could be related to the preparation procedure. In the PUL/SA systems alginate was mixed with pullulan to form a homogeneous structure and the Ca^{2+} addition, to achieve the crosslinking, was probably less effective to allow the formation of alginate egg box structure. This caused pullulan and alginate chain entanglements, resulting in less structured gelation (crosslinking). On the contrary, when alginate (non-blended with other polymers) was used to coat the nanofibers, the crosslinking was more effective, and alginate could freely form egg-box structure giving a tighter structure. Differences in the supposed alginate organization could be at the basis of protein release: where the polymeric network was tighter, as for PUL/CA coated SA/PL scaffolds, the protein diffusion was slower, while in PUL/SA-PL systems, proteins could easily escape from the polymer network giving a faster release.

3.6. In vitro fibroblast adhesion and proliferation

Fig. 11 shows the viability (%) of fibroblasts grown onto scaffolds for 3 and 6 days. The control, considered 100% was the growth medium and in this condition the growth was considered as optimal (standard) (fibroblasts seeded onto well bottom in growth medium).

After 3 days, PUL/SA scaffolds were characterized by a cell growth

significantly lower than that of the substrate in standard condition, and the PL loading did not significantly increase cell adhesion and proliferation. After 6 days, fibroblast proliferation onto PUL/SA scaffolds was significantly higher than that after 3 days of growth and the presence of PL did not further enhance cell proliferation.

As for coated nanofibers, analogously to PUL/SA scaffolds, PUL/CA coated SA scaffolds were characterized by a cell growth significantly lower than that obtained in standard condition independently of PL loading. After 6 days, fibroblast proliferation onto PUL/SA scaffolds was significantly higher than that after 3 days of growth. Moreover, the presence of PL again did not further enhance cell proliferation. The different type of PL loading determined a significant increase of cell adhesion after 3 days proliferation for PUL/CA coated SA scaffolds, while after 6 days of growth, the presence of PL leveled out the difference in cell growth.

CLSM analysis (Fig. 12) confirmed the adhesion and proliferation results. Fibroblasts appeared confluent onto scaffolds independently of scaffold types and PL loading. However, when the cell substrates adhered and proliferated onto PL unloaded scaffolds, fibroblasts presented stretched cytoskeletons resembling fusiform shape of mature fibroblasts and a cell alignment typical of fibroblast substrates [35]. On the contrary, when PL was loaded into the scaffolds, fibroblasts lost the features typical of aligned fusiform cells and assumed a randomly oriented conformation. In literature, it is described that the presence of growth factors (TGF and FGF) enhances fibroblast-to-myofibroblast transition [36]. The transition of fibroblasts towards cells capable to migrate should enhance wound healing process, since myofibroblasts are key players in contraction of wound bed and in the moving closer of injured edges. Moreover, these have a crucial role in the remodelling and maturation phase [37]. No difference in term of adhesion and proliferation was determined by both PL loaded scaffolds although the release profiles were different. This is probably due to the high potency of GF pool contained in PL so both the systems seem to reach the trigger concentration value to stimulate fibroblasts.

4. Conclusion

Nanofibrous scaffolds of PUL and SA combine the advantages of SA, as biopolymer, with improved physical structure, providing an advantageous approach for skin regeneration. Two preparation approaches have been used to load PL in the scaffolds, as component of the polymeric matrix, to be electrospun, or as coating component, to cover the previously prepared electrospun membranes. These mainly affected the fiber dimension of the scaffolds which resulted bigger in the coated systems. On the contrary, the mechanical properties, especially in PL loaded systems, were deeply affected by PL loading and the coated systems (PUL/CA coated SA) were characterized by stiffness higher than that of matrix scaffolds (PUL/SA). These opposite behaviours were conceivably caused by the coating layer based on SA gelled with Ca^{2+} with a different consistency with respect to PUL-CA based core. Anyhow, these differences in fiber dimension and in mechanical properties were not crucial for fibroblast adhesion and proliferation. On the contrary, the presence of PL was responsible for different fibroblast conformation and orientation. In particular PL seems to lead fibroblast random orientation compatible to a fibroblast-to-myofibroblast transition that could be effective to enhance wound healing.

Acknowledgement

The authors wish to thank Dr. P. Vaghi (Centro Grandi Strumenti, University of Pavia) for CLSM, Dr. I. Tredici (CISRiC, University of Pavia, Italy) for SEM measurements.

Declaration of Competing Interest

The authors declare that there are no conflicts of interest

References

[1] R. Augustine, N. Kalarikkal, S. Thomas S, Advancement of wound care from grafts to bioengineered smart skin substitutes, Prog. Biomat. 3 (2014) 103–113.
[2] J. Li, J. Chen, R. Kirsner, Pathophysiology of acute wound healing, Clin. Dermatol. 25 (2007) 9–18.
[3] J.M. Reinke, H. Sorg, Wound repair and regeneration, Eur. Surg. Res. 49 (2012) 35–43.
[4] C.K. Sen, G.M. Gordillo, S. Roy, R. Kirsner, L. Lambert, T.K. Hunt, F. Gottrup, G.C. Gurtner, M.T. Longaker, Human skin wounds: a major and snowballing threat to public health and the economy, Wound Repair Regen. 17 (2009) 763–771.
[5] S.A. Eming, P. Martin, M. Tomic-Canic, Wound repair and regeneration: mechanisms, signaling, and translation, Sci. Transl. Med. 6 (2014) 265–270.
[6] K. Okuda, T. Kawase, M. Momose, Platelet-rich plasma contains high levels of platelet-derived growth factor and transforming growth factor-beta and modulates the proliferation of periodontally related cells in vitro, J. Periodontol. 74 (2003) 849–857.
[7] E. Ranzato, M. Patrone, L. Mazzucco, B. Burlando, Platelet lysate stimulates wound repair of HaCaT keratinocytes, Br. J. Dermatol. 159 (2008) 537–545.
[8] R.E. Backly, V. Ulivi, L. Tonachini, R. Cancedda, F. Descalzi, M. Mastrogiacomo, Platelet lysate induces in vitro wound healing of human keratinocytes associated with a strong proinflammatory response, Tissue Eng. Part A 17 (2011) 1787–1800.
[9] D.P. Mohanan, R. Augustine, N. Kalarikkal, E.K. Radhakrishnan, S. Thomas, Electrospun matrices for biomedical applications: recent advances, in: N. Kalarikkal, R. Augustine, O.S. Oluwafemi, S. Thomas (Eds.), Nanomedicine and tissue engineering: state of the art and recent trends, CRC Press, 2016, p. 365–90.
[10] K. Ghosal, K.C. Agatemor, Z. Špitálsky, S. Thomas, E. Kny, Electrospinning tissue engineering and wound dressing scaffolds from polymer-titanium dioxide nanocomposites, Chem. Eng. J. 358 (15) (2019) 1262–1278.
[11] K. Ghosal, C. Agatemor, N. Tucker, E. Kny, S. Thomas, Electrical spinning to electrospinning: a brief history RSC soft matter 7 (2018) 1–23, in: K. Ghosal, E. Kny, S. Thomas (Eds.), Electrospinning: basic research to commercialization, Royal Society of Chemistry.
[12] S. Krause, D.R. Paul, S. Newman, Polymer-Polymer Compatibility, Polymer Blends, Academic Press, New York, 1978, p. 1.
[13] G.R. Mitchell, K. Ahn, F.J. Davis, The potential of electrospinning in rapid manufacturing processes, Virt. Phys. Prototyp. 6 (2011) 63–77.
[14] M.P. Prabhakaran, L. Ghasemi-Mobarakeh, S. Ramakrishna, Electrospun composite nanofibers for tissue regeneration, J. Nanosci. Nanotechnol. 11 (2011) 3039–3057.
[15] S. Thomas, Y. Grohens, N. Ninan, Nanotechnology applications for tissue engineering nanotechnology applications for tissue engineering, Elsevier, 2015, pp. 1–315.
[16] R.F. Pereira, C.C. Barrias, P.L. Granja, P.J. Bartolo, Advanced biofabrication strategies for skin regeneration and repair, Nanomedicine 8 (2013) 603–621.
[17] R.S. Singh, G.K. Saini, J.F. Kennedy, Pullulan: Microbial sources, production and applications, Carbohydr. Polym. 73 (2008) 515–531.
[18] X.B. Sun, D. Jia, W.M. Kang, B.W. Cheng, Y.B. Li, Research on electrospinning process of pullulan nanofibers, Appl. Mech. Mater. Trans. Tech. Publ. (2013).
[19] A.C. Mendes, K. Stephansen, I.S. Chronakis, Electrospinning of food proteins and polysaccharides, Food Hydrocoll. 68 (2017) 53–68.
[20] C.A. Bonino, M.D. Krebs, C.D. Saquing, S.I. Jeong, K.L. Shearer, E. Alsberg, Electrospinning alginate-based nanofibers: from blends to crosslinked low molecular weight alginate-only systems, Carbohydr. Polym. 85 (2011) 111–119.
[21] N. Reddy, Y. Yang, Innovative Bio Bers from Renewable Resources, Springer, New York, 2015.
[22] C. Caramella, F. Ferrari, M.C. Bonferoni, M. Ronchi, P. Colombo, Rheological properties and diffusion dissolution behaviour of hydrophilic polymers, Boll. Chim. Farm. 128 (1989) 298–302.
[23] G. Sandri, S. Rossi, M. C. Bonferoni, D. Miele, A. Faccendini, E. Del Favero, E. Di Cola, A. Icaro Cornaglia, C. Boselli, T. Luxbacher, L. Malavasi, L. Cantu', F. Ferrari, Chitosan/glycosaminoglycan scaffolds for skin reparation, submitted to Carb. Polym.
[24] B. Vigani, S. Rossi, G. Milanesi, M.C. Bonferoni, G. Sandri, G. Bruni, F. Ferrari, Electrospun alginate fibers: mixing of two different poly(ethylene oxide) grades to improve fiber functional properties, Nanomaterials 8 (2018) 971.
[25] A. Koski, K. Yim, S. Shivkumar, Effect of molecular weight on fibrous PVA produced by electrospinning, Mater. Lett. 58 (2004) 493–497.
[26] P. Gupta, C. Elkins, T.E. Long, G.L. Wilkes, Electrospinning of linear homopolymers of poly(methyl methacrylate): exploring relationships between fiber formation, viscosity, molecular weight and concentration in a good solvent, Polymer 46 (2005) 4799–4810.
[27] M.G. McKee, C.L. Elkins, T.E. Long, Influence of self-complementary hydrogen bonding on solution rheology/electrospinning relationships, Polymer 45 (2004) 8705–8715.
[28] M.G. McKee, M.T. Hunley, J.M. Layman, T.E. Long, Solution rheological behaviour and electrospinning of cationic polyelectrolytes, Macromolecules 39 (2006) 575–583.
[29] C. Drew, X.Y. Wang, L.A. Samuelson, J. Kumar, The effect of viscosity and filler on electrospun fiber morphology, J. Macromol. Sci. A. A40 (2003) 1415–1422.
[30] L. Huang, K. Nagapudi, R.P. Apkarian, E.L. Chaikof, Engineered collagen-PEO nanofibers and fabrics, J. Biomater. Sci. Polym. 12 (2001) 979–993.
[31] N. Bhardwaj, S.C. Kundu, Electrospinning: a fascinating fiber fabrication technique, Biotechnol. Adv. 28 (2010) 325–347.
[32] S.C. Liu, R. Li, P.M. Tomasula, A.M. Sousa, L. Liu, Electrospun food-grade ultrafine fibers from pectin and pullulan blends, Food Sci. Nutr. 7 (2016) 636–642.

[33] S. Saber-Samandari, H.O. Gulcan, S. Saber-Samandari, M. Gazi, Efficient removal of anionic and cationic dyes from an aqueous solution using Pullulan-graft-poly-acrylamide porous hydrogel, Water Air Soil Pollut. 225 (2014) 2177.
[34] A. Tojeira, D.C. Vaz, A. Mendes, P. Bártolo, Preparation and characterization of films based on alginate and aloe vera, Int. J. Polym. Anal. Charact. 16 (2011) 449–464.
[35] R. Li, T.F. Balagam, P.P. He, O.A. Lee, H. Igoshin, Levine, on the mechanism of long-range orientational order of fibroblasts, Proc. Natl. Acad. Sci. USA 114 (2017) 8974–8979.
[36] R.C. Stone, I. Pastar, N. Ojeh, Epithelial-mesenchymal transition in tissue repair and fibrosis, Cell Tissue Res. 3 (2016) 495–506.
[37] B. Hinz, S.H. Phan, V.J. Thannickal, A. Galli, M.L. Bochaton-Piallat, G. Gabbiani, The myofibroblast: one function, Multiple Origins. Am. J. Pathol. 170 (2007) 1807–1816.